STEM CELLS TRANSLATIONAL MEDICINE®

TISSUE ENGINEERING AND REGENERATIVE MEDICINE

Postinfarction Functional Recovery Driven by a Three-Dimensional Engineered Fibrin Patch Composed of Human Umbilical Cord Blood-Derived Mesenchymal Stem Cells

SANTIAGO ROURA,[a,*] CAROLINA SOLER-BOTIJA,[a,*] JULI R. BAGÓ,[b,c,*] AIDA LLUCIÀ-VALLDEPERAS,[a] MARCO A. FÉRNANDEZ,[d] CAROLINA GÁLVEZ-MONTÓN,[a] CRISTINA PRAT-VIDAL,[a] ISAAC PEREA-GIL,[a] JERÓNIMO BLANCO,[b,c] ANTONI BAYES-GENIS[a,e,f]

Key Words. Myocardial infarction • Umbilical cord blood • Mesenchymal stem cells • Fibrin • Patch • Cardiac function

[a]Heart Failure and Cardiac Regeneration Research Program and [d]Flow Cytometry Facility, Germans Trias i Pujol Health Science Research Institute, Badalona, Spain; [b]Cell Therapy Group, Institute for Advanced Chemistry of Catalonia, Barcelona, Spain; [c]Biomedical Research Networking Center on Bioengineering, Biomaterials and Nanomedicine, Zaragoza, Spain; [e]Cardiology Service, University Hospital, Germans Trias i Pujol, Badalona, Spain; [f]Department of Medicine, Universitat Autònoma de Barcelona, Barcelona, Spain

[*]Contributed equally.

Correspondence: Antoni Bayes-Genis, M.D., Ph.D., Heart Failure and Cardiac Regeneration Research Program, Cardiology Service, Hospital Universitari Germans Trias i Pujol, Crta. Canyet, s/n, Badalona, Barcelona, 08916 Spain. Telephone: 34-93-497-3743; E-Mail: abayes.germanstrias@gencat.cat

Received November 13, 2014; accepted for publication April 17, 2015; published Online First on June 23, 2015.

1066-5099/2015/$20.00/0

http://dx.doi.org/10.5966/sctm.2014-0259

ABSTRACT

Considerable research has been dedicated to restoring myocardial cell slippage and limiting ventricular remodeling after myocardial infarction (MI). We examined the ability of a three-dimensional (3D) engineered fibrin patch filled with human umbilical cord blood-derived mesenchymal stem cells (UCBMSCs) to induce recovery of cardiac function after MI. The UCBMSCs were modified to coexpress luciferase and fluorescent protein reporters, mixed with fibrin, and applied as an adhesive, viable construct (fibrin-cell patch) over the infarcted myocardium in mice (MI-UCBMSC group). The patch adhered well to the heart. Noninvasive bioluminescence imaging demonstrated early proliferation and differentiation of UCBMSCs within the construct in the postinfarct mice in the MI-UCBMSC group. The implanted cells also participated in the formation of new, functional microvasculature that connected the fibrin-cell patch to both the subjacent myocardial tissue and the host circulatory system. As revealed by echocardiography, the left ventricular ejection fraction and fractional shortening at sacrifice were improved in MI-UCBMSC mice and were markedly reduced in mice treated with fibrin alone and untreated postinfarction controls. In conclusion, a 3D engineered fibrin patch composed of UCBMSCs attenuated infarct-derived cardiac dysfunction when transplanted locally over a myocardial wound. STEM CELLS TRANSLATIONAL MEDICINE *2015;4:956–966*

SIGNIFICANCE

Ischemic heart failure (HF) is the end stage of many cardiovascular diseases, including myocardial infarction. The only definitive treatment for HF is cardiac transplant, which is hampered by limited number of heart donors and graft rejection. In recent times, cellular cardiomyoplasty has been expected to repair infarcted myocardium by implantation of different sources of stem or progenitor cells. However, low cell survival and myocardial implantation rates have motivated the emergence of novel approaches with the objective of generating graftable cell-based implants. Here, the potential of 3D engineered fibrin-umbilical cord blood-derived mesenchymal stem cells patches is shown to significantly recover lost general functions in post-infarcted mice.

INTRODUCTION

A large amount of research has focused on restoring myocardial cell slippage and limiting ventricular remodeling after myocardial infarction (MI) [1, 2]. Cellular cardiomyoplasty aims to generate new myocardial tissue and blood vessels by using cells with regenerative potential [3–6]. However, the cell survival is low in the harsh postinjury milieu; thus, the benefits of cardiomyoplasty for the recovery of cardiac function have been modest at best. This has led to the development of newly designed cell scaffolds or "patches" for myocardial implantation, in which cells with a regenerative capacity are combined with biological and synthetic materials that can also be supplemented with growth or differentiation factors to generate graftable bioimplants [7–10]. The behavior of cells within biomaterial implants can be monitored with tools, such as bioluminescence imaging (BLI), that provide noninvasive, real-time information [11, 12].

Despite significant advances in myocardial revascularization and reperfusion, effective promotion

of angiogenesis is still a challenge for cardiac regeneration [13–15]. Thus, there is great interest in the identification of new types of vascular precursors. We recently reported that human umbilical cord blood (UCB) is a source of multipotent mesenchymal stem cells (MSCs) [16–18]. After genetic modification, UCBMSCs were implanted in live animals and noninvasively monitored, which showed differentiation toward the endothelial lineage and the induction of new vasculature [19].

In the present study, we examined the capacity of a three-dimensional (3D), engineered fibrin patch, filled with UCBMSCs, to induce functional vascular connections with the host myocardium and improve cardiac function after MI in mice.

Materials and Methods

Cell Culture and Baseline Characterization

Human UCBMSCs were isolated and cultured as described previously [16, 17]. The cells were maintained in α-minimal essential medium (Sigma-Aldrich, St. Louis, MO, http://www.sigmaaldrich.com) supplemented with 10% fetal bovine serum (FBS), 1 mM L-glutamine, and 1% penicillin/streptomycin (Gibco, Grand Island, NY, http://www.lifetechnologies.com).

The cell surface expression of CD29, CD34, CD44, CD45, CD106, and CD166 was assessed in 3×10^5 cells incubated with monoclonal antibodies (mAbs) (10 μl of anti-CD29 phycoerythrin [PE]-conjugated, anti-CD44 fluorescein isothiocyanate [FITC]-conjugated, anti-CD106 FITC-conjugated, and anti-CD166 PE-conjugated; 5 μl of anti-CD45 peridinin chlorophyll protein complex-conjugated and anti-CD34 PE-conjugated; BD Pharmingen, San Diego, CA, http://www.bdbiosciences.com) in 100-μl phosphate-buffered saline (PBS) (Sigma-Aldrich) containing 1% FBS for 20 minutes at room temperature. Data were acquired on an LSRFortessa flow cytometer (BD Biosciences, San Diego, CA, http://www.bdbiosciences.com), and IgG isotype controls were used to set gate boundaries for positive cells. Data analysis was performed with FlowJo software (FlowJo, LLC, Ashland, OR, http://www.flowjo.com).

Genetic Modification of UCBMSCs

Lentiviral production was performed as described previously [11, 20]. The UCBMSCs were cotransduced (2×10^6 transducing units per milliliter, multiplicity of infection = 21, 48 hours) with the following lentiviral vectors: CMVp-RLuc-mRFP1, which contains a chimeric construct of the *Renilla reniformis* luciferase (RLuc) reporter gene and monomeric red fluorescent protein (mRFP1) in a PHR lentiviral vector under transcriptional control of the cytomegalovirus (CMV) promoter [21]; and CD31p-PLuc-eGFP, a fusion reporter vector composed of *Photinus pyralis* luciferase (PLuc) and enhanced green fluorescent protein (eGFP) coding regions under the transcriptional control of the 0.25-kb NorI/PstI fragment of the human CD31 promoter, which has higher transcriptional activity in endothelial cells than in monocytic cells [22]. Cells expressing mRFP1 were selected by fluorescence-activated cell sorting.

Cell Viability Analysis

To determine the cell viability in the fibrin patches, the Live/Dead viability/cytotoxicity kit (Invitrogen, Carlsbad, CA, http://www.invitrogen.com) was used according to the manufacturer's instructions. In brief, fibrin patches loaded with 1.5×10^6 cells and cultured for 24 hours under standard culture conditions were washed in PBS before staining. The patch constructs were then analyzed with a confocal microscope (Axio-Observer Z1; Carl Zeiss, Jena, Germany, http://www.zeiss.com), and tiles-stitching image postprocessing was applied (Zen Blue software; Carl Zeiss).

Animal Studies

The Animal Experimentation Unit Ethical Committee of the Catalan Institute of Cardiovascular Sciences (ICCC) approved the animal studies, which complied with the guidelines concerning the use of animals in research and teaching, as defined by the *Guide for the Care and Use of Laboratory Animals* (NIH Publication no. 80-23, revised 1996). All procedures were also performed in accordance with both national and European legislation: Spanish Royal Decree RD 53/2013 and EU Directive 2010/63/EU for the protection of animals used for research experimentation and other scientific purposes.

Experimental Groups

The study was performed on 35 female SCID mice (weight, 20–25 g; Charles River Laboratories, Wilmington, MA, http://www.criver.com). The mice were randomly distributed to the following groups: control-MI (n = 8), MI treated with fibrin alone (MI-fibrin; n = 8), and MI treated with implantation of the fibrin-cell patches (MI-UCBMSC; n = 13). A sham group without MI, but with implantation of the fibrin-cell patches was also included (sham-UCBMSC; n = 6). The global mortality in the experiment was 5.7%, 25% in the control-MI group and 0% in the other groups; 2 of 35 mice died as a result of surgery.

MI Model and Delivery of the Fibrin-Cell Patch

MI was achieved as described previously [19]. In brief, the mice were anesthetized with a mixture of O_2/isoflurane (2%) (Baxter International Inc., Deerfield, IL, http://www.baxter.com), intubated, and mechanically ventilated (90 breaths per minute, 0.1 ml tidal volume) using a SAR830/AP small animal ventilator (CWE, Inc., Ardmore, PA, http://www/cwe-inc.com). An anterior thoracotomy was performed, and the proximal left anterior descending (LAD) coronary artery was occluded using a 7-0 silk suture. The sham-UCBMSC mice were prepared in the same manner except that the LAD coronary artery was not occluded before implantation of the fibrin-cell patches.

To generate the adhesive constructs, Tissucol solution (8 μl; Baxter International) with 1.5×10^6 transduced cells or culture medium was mixed with 8 μl of thrombin solution for jellification (Tissucol Duo; Baxter International). The fibrin and cells were maintained under standard culture conditions for 24 hours. Fibrin patches with or without cells were implanted after MI induction and in the sham-UCBMSC mice using Glubran 2 surgical glue (Cardiolink Corp., Levittown, NY, http://www.cardiolink.net), which fulfills the required safety and compatibility standards for experimental animals and human use [23, 24], to seal the edges of the patch to the myocardium. The mice were sacrificed 4 weeks after the operation. Using cardioplegic solution, the hearts were arrested in diastole [25] and then excised, fixed in 10% formalin solution (Sigma-Aldrich), cryopreserved in 30% sucrose in PBS, embedded in Tissue Tek O.C.T. (Sakura Finetek Europe B.V., Alphen aan den Rijn, The Netherlands, http://www.sakura-fintek.com), and snap-frozen in liquid nitrogen-cooled isopentane for histological analysis.

Noninvasive BLI

Monitoring of activation of the CD31 promoter or cell number was performed as previously described [11]. The mice were injected either intraperitoneally with 150 μl of luciferin (PLuc substrate; 16.7 mg/ml in physiological serum; Caliper Life Sciences, PerkinElmer, Hopkinton, MA, http://www.perkinelmer.com) or through the lateral tail vein with 25 μl of benzyl coelenterazine (RLuc substrate; 1 mg/ml in 50% vol/vol propylene glycol/ethanol; Nanolight Technology, Prolume Ltd., Pinetop, AZ, http://www.nanolight.com). PLuc and RLuc activities were monitored under the IVIS Spectrum in vivo photon counting device (Caliper Life Sciences). Images of Pluc and Rluc were captured on consecutive days during a 3-week period. The images were quantified in units of maximum photons per second per square centimeter per steradian (p/s/cm^2/sr) and analyzed using Living Image 3.10 software (Caliper Life Sciences). The final recorded light fluxes were expressed as photon counts after subtracting the background.

Analysis of Cardiac Function

Cardiac function was assessed by echocardiography using an 18–38-MHz linear-array transducer with a digital ultrasound system (Vevo 2100 Imaging System; VisualSonics, Toronto, ON, Canada, http://www.visualsonics.com). Measurements were taken at baseline, 2 days after MI, and 4 weeks after the operation. The investigators were unaware of the treatment groups. Standard parasternal long-axis and short-axis views were obtained in B-mode and M-mode. The left ventricle (LV) end-diastolic diameter (LVEDD) and LV end-systolic diameter (LVESD) were quantified and the LV ejection fraction (LVEF) was calculated according to the Teichholz equation [26].

Fluorescence Angiography

Ten minutes before sacrifice, 200 μl of FITC-dextran (10 mg/ml; Sigma-Aldrich) were injected through the lateral tail vein of the anesthetized (2% O_2/isoflurane) mice. After removal and fixation for histologic examination, the tissue was sliced and imaged using a TCS SP2 laser confocal microscope (Leica, Heerbrugg, Switzerland, http://www.leica.com) to analyze the green fluorescent microvascular structures connecting the myocardium with the implanted fibrin-cell patches.

Morphometric and Immunohistochemical Examination

The hearts were cross-sectioned from the apex to the base (10-μm-thick sections spaced every 300 μm). Eight serial cryosections per mouse were stained with Masson's trichrome (collagen, blue; myocardium, red) for morphometry. To evaluate the infarct thickness, the LV wall thickness was measured at the thinnest portion and at the border zones of the infarction. Three measurements were made per section to determine the posterior wall thickness distal to the infarction. The mean value of the eight sections was calculated for the thickness parameters. The infarct size volume, expressed as a percentage of the total LV wall volume, was calculated by summing the partial scar volumes between sections. All sections were examined (blindly) and photographed using a TL RCI stereoscope (Leica).

Immunostaining was performed on the fibrin-cell patch after 24 hours' incubation to determine the expression levels of CD31 at in vivo implantation. The fibrin-cell patch was incubated with an anti-CD31 antibody (0.8 μg/ml; Abcam, Cambridge, U.K., http://www.abcam.com) for 48 hours at 4°C to ensure its access to the innermost cells. In these experiments, the cell cytoplasm was counterstained with phalloidin Atto 488-conjugated (Sigma-Aldrich). Additional immunoanalysis was performed on cryosections to detect CD31 and cardiac troponin I using specific mAb (0.8 μg/ml and 2 μg/ml, respectively; Abcam). The vessel area was assessed in sections stained with biotinylated GSLI B4 isolectin (Vector Laboratories, Burlingame, CA, http://www.vectorlabs.com). Nuclei were counterstained with Hoechst 33342 (Sigma-Aldrich). The images were captured under a laser confocal microscope (Axio-Observer Z1, Zeiss). Quantitative histological measurements were made using ImageJ analysis software (NIH, Bethesda, MD).

Statistical Analysis

The significance of the bioluminescent signal was evaluated by analysis of variance (ANOVA) using time (baseline, just after MI, and 30 days after) and treatment (sham-UCBMSC, control-MI, MI-fibrin, and MI-UCBMSC groups) as factors. A Greenhouse-Geisser correction was applied. The vessel density, survival rate, and morphometric data were assessed using one-way ANOVA. To evaluate the functional parameters, the homogeneity of the MIs in all the groups was first determined comparing the baseline and post-MI LVEF and LV fractional shortening (FS) by ANOVA using time (baseline, post-MI) and treatment as factors. The LVEF and LVFS differentials between the baseline and presacrifice values were evaluated using one-way ANOVA. Pairwise comparisons between groups were made using Tukey post hoc analysis for multiple comparisons. The results are presented as the mean $\pm$ SD; $p < .05$ was considered significant. All analyses were performed using SPSS Statistics, version 19.0.0.1 (SPSS software, IBM Corp., Armonk, NY, http://www-01.ibm.com/software/analytics/spss/).

RESULTS

In these experiments, we sought to track the survival and differentiation of UCBMSCs toward endothelial lineage in vivo using noninvasive BLI. In order to determine whether established cell cultures were pure populations of MSCs, we first assessed the expression of cell surface antigens by flow cytometry. These analyses ensured that UCBMSC cultures were strictly homogeneous and did not show baseline expression of either endothelial (CD34 negative) or hematopoietic (CD45 negative) cell traits (Fig. 1). The cells were then transduced with a CMVp-RLuc-mRFP1 lentiviral vector, in which the chimeric protein RLuc-mRFP1 was expressed under the regulation of the constitutively active CMV promoter (as a reporter of cell number). Positively transduced cells were separated by fluorescence-activated cell sorting and then transduced with a second lentiviral vector, CD31p-PLuc-eGFP, in which the chimeric protein Pluc-eGFP was expressed under the control of the inducible promoter of the human CD31 gene (a protein expressed in the endothelial cell lineage and used as a marker of vascular differentiation). This strategy allowed monitoring of the ratio of light produced by CD31 promoter-regulated PLuc relative to that produced by the internal standard, the CMV promoter-regulated RLuc. Thus, changes in cellular differentiation could be evaluated irrespective of changes in cell number.

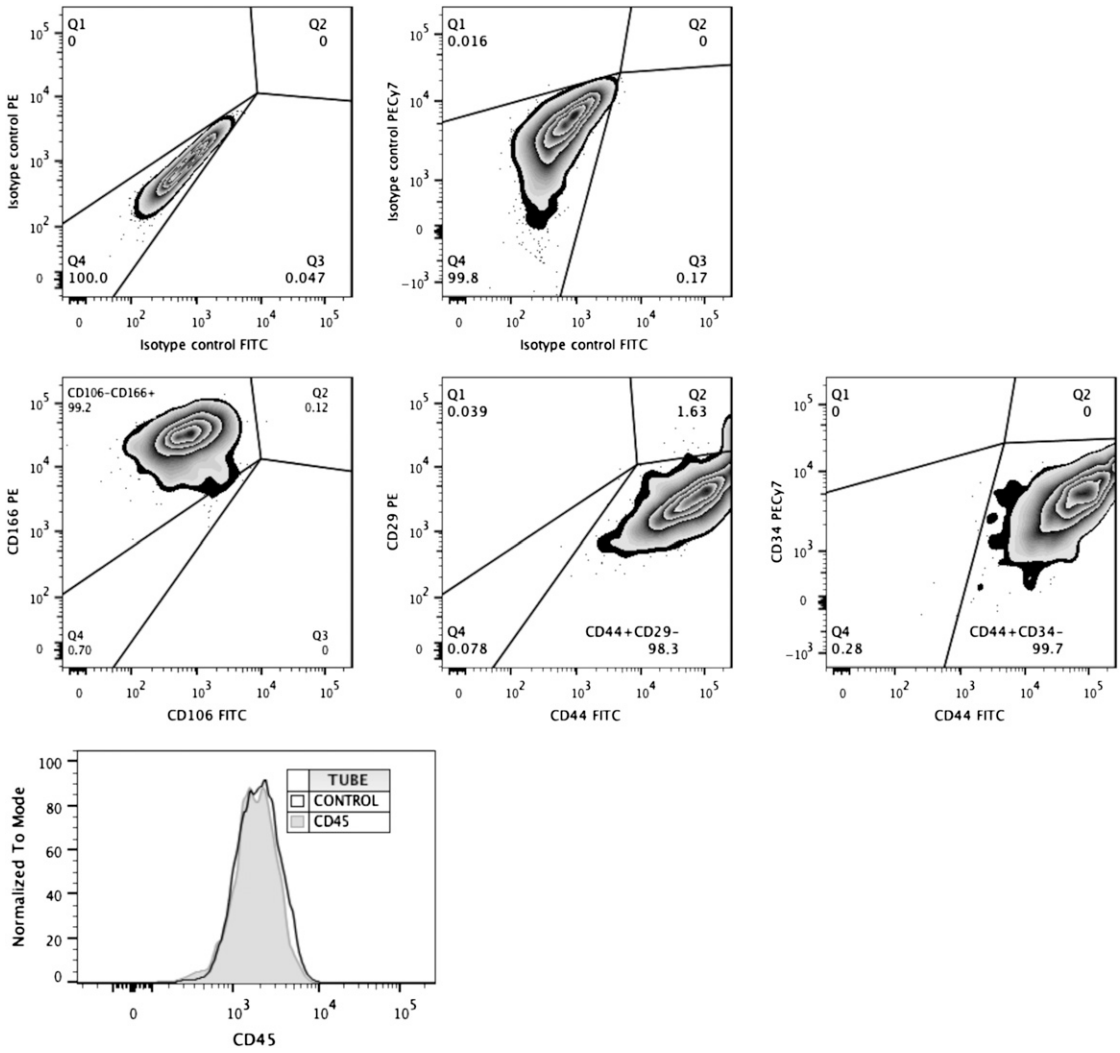

Figure 1. Analysis of phenotypic traits exhibited by primary umbilical cord blood mesenchymal stem cell (UCBMSC) cultures. Representative flow cytometric data showing expression levels of MSC-specific, endothelial-specific (middle), and hematopoietic-specific (bottom) cell surface markers by established cultures of UCBMSCs. Gate boundaries were performed using isotype controls (top; overlaid with marker in bottom plot), and dead cells were excluded using viability dye (data not shown). Abbreviations: FITC, fluorescein isothiocyanate; PE, phycoerythrin.

Double-transduced cells were subsequently mixed with fibrin, and we assessed the viability and differentiation status of the 3D patch before in vivo implantation. The cells remained highly viable in the construct, with viable cells having a fluorescence intensity (green) of 74% and dead cells (red) one of only 26% as tested using the Live/Dead viability/cytotoxicity assay (Invitrogen; Fig. 2A, 2A′). Also, no baseline and/or induction of CD31 protein expression was corroborated in vitro (Fig. 2B). Therefore the resulting engineered construct was fixed over the infarcted area in a mouse model of acute MI. We observed good attachment of the patch to the heart through macroscopic analysis (Fig. 3A). Bioluminescence and fluorescence images were taken from the explanted heart of a postinfarcted mouse implanted with a fibrin-cell patch (MI-UCBMSC group). Luciferase, eGFP, and mRFP1 signals were detected in excised hearts, indicating the retention and local presence of the implanted cells after sacrifice (Fig. 3A). Weekly quantification of photon emission from the hearts during a 3-week period revealed a 2.3-fold increase in the PLuc/RLuc ratio relative to that at implantation time, indicative of CD31 promoter activation among the surviving cells (p = .003; Fig. 3B, 3C). The PLuc/RLuc ratio did not change over time in the sham-treated mice (Fig. 3C; supplemental online Fig. 1). Moreover, in the MI-UCBMSC group, CMV-regulated RLuc activity increased at week 1 relative to the activity at implantation (1.5-fold; p = .045) and later decayed to approximately 12% of the initial value (Fig. 3D). Using a previously reported correlation between RLuc emission and cell number for our lentivirally cotransduced cells [19], we estimated that the fraction of viable cells within the patch at 3 weeks after implantation, relative to that at implantation, was 3%. In the case of the sham-treated mice, the number of RLuc expressing cells steadily decreased after implantation (Fig. 3D). These results suggest that MI-derived factors might induce early proliferation and differentiation of cells within the fibrin patch.

Histological analyses of cross-sections of the excised hearts bearing fibrin-cell patches corroborated that the constructs were well adhered to the mouse myocardium, covering the infarcted scar. In concordance with the BLI findings, we detected the

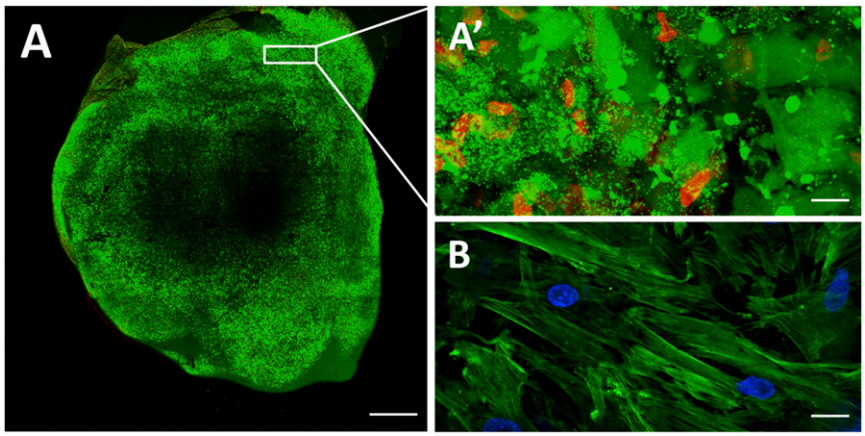

Figure 2. Assessment of cell viability and differentiation status in the fibrin patch before in vivo implantation. **(A):** Representative image showing cell viability in a fibrin patch loaded with umbilical cord blood mesenchymal stem cells (UCBMSCs) and cultured for 24 hours in standard culture conditions. Viable cells are shown in green and dead cells in red, as performed using the Live/Dead viability/cytotoxicity kit (Invitrogen). **(A′):** Magnification of a selected peripheral area with a predominance of viable cells (green). **(B):** Fibrin patch immunostaining showing absence of CD31 expression (red) in UCBMSCs. Cell cytoplasm and nucleus were counterstained with Atto 488-phalloidin (green) and 4′,6-diamidino-2-phenylindole, respectively. Scale bars = 1 mm **(A)** and 20 μm **(A′, B)**.

presence of red and green fluorescence (on activation of the CD31 promoter-regulated PLuc-eGFP reporter, indicating positive expression of CD31 protein) human cells within the construct (Fig. 4C). Some doubly labeled red and green fluorescent UCBMSCs, which expressed CD31 protein, exhibited endothelial cell morphology and were arranged, forming vessel-like structures within the fibrin-cell patch in the MI-UCBMSC mice (Fig. 4A–4D, 4F). Additional analysis of vascular structures by GSLI B4 staining (Vector Laboratories) did not reveal differences in vessel density in the distal myocardium or in the border of MI regions among the groups (Fig. 4E). After injection of high-molecular-weight FITC-dextran through the lateral tail vein of live mice, fluorescent angiography was performed to visualize the formation of new vascular structures, integrated by human mRFP1$^+$ cells and connected to the host circulatory system, at the interface between the infarcted myocardium wound and the engrafted fibrin-cell patch (Fig. 4G). In general, no implanted cells (i.e., mRFP1$^+$ cells) were found in the myocardium of the MI-UCBMSC or sham-treated mice, indicating an absence of migration from the patch to the underlying heart.

The results from the morphometric analyses of the heart cross-sections through the infarcted myocardium 4 weeks after surgery showed that the LV scar thickness (control-MI, 0.16 $\pm$ 0.08 mm; MI-fibrin, 0.24 $\pm$ 0.11 mm; and MI-UCBMSC, 0.24 $\pm$ 0.17 mm; p = . 476) and volume (control-MI, 36.32% $\pm$ 12.40%; MI-fibrin, 40.29% $\pm$ 15.23%; and MI-UCBMSC, 35.21% $\pm$ 10.96%; p = .836) were similar in the three groups of infarcted mice (supplemental online Fig. 2).

Functional analyses were performed to determine whether post-MI implantation of the adhesive fibrin-cell patch had a positive effect on cardiac function (Table 1). First, to ensure homogeneity of the surgical procedure in the studied groups (control-MI, MI-fibrin, and MI-UCBMSC), a Greenhouse-Geisser analysis was applied to assess MI size (comparing baseline and post-MI LVEF and LVFS) [27, 28]. These comparisons revealed no statistically significant differences among the groups (p = .23 and p = .32 for LVEF and LVFS, respectively; data not shown). LVEF and LVFS were also calculated as differentials between the values at 30 days postoperatively and those at baseline and compared among the MI groups (Table 2). This analysis showed that evolution of both cardiac function parameters was significantly different statistically between the MI-UCBMSC and control-MI/MI-fibrin mice. In the MI-UCBMSC group, calculations of ΔLVEF revealed a clinically relevant ($<-10\%$) value ($-8.7\% \pm 8.8\%$). In particular, 73% of the mice treated with the patches bearing cells had ΔLVEF $<-10\%$. In contrast, in the control-MI and MI-fibrin groups, 100% and 86% of the mice had ΔLVEF $\geq -10\%$ ($-21.4\% \pm 7.7\%$ and $-23.1\% \pm 23\%$, respectively). Additional global analysis confirmed that the ΔLVEF of the MI-UCBMSC group was significantly different from that of the control-MI and MI-fibrin groups (p = .03; Fig. 5). Similar results were obtained in the LVFS analysis: only 20% of the MI-UCBMSC and 83% of the control-MI and 86% of the MI-fibrin mice had a ΔLVFS $\geq -10\%$ ($-6.2\% \pm 7\%$, $-13.6\% \pm 5.1\%$ and $-15.1\% \pm 5\%$, respectively; Table 2). The differences in ΔLVFS were also statistically significant when compared globally (p = .013; Fig. 5).

Discussion

Although the residual scar size after acute MI has shrunk owing to recent innovations, such as evidence-based medicine (aspirin, β-blockers, angiotensin-converting enzyme inhibitors), and the incorporation of primary percutaneous coronary interventions, a portion of the heart still becomes hypokinetic or akinetic. Cell-based therapies have been proposed for functional tissue replacement in these patients [6, 29–31]. However, this requires efficient delivery and survival of large numbers of cells within the injured heart to be effective, and this poses a major challenge [6].

In general, strategies based on the delivery of cells with regenerative capacity are feasible and safe; however, they have exhibited only modest benefits in the recovery of cardiac function. These limited effects probably result from the adverse mechanical stress and hypoxic conditions present in the myocardium after infarct [32]. The injection of regenerative cells into the infarcted area frequently results in low cell engraftment within the myocardial scar [6, 33–35]. Furthermore, based on our

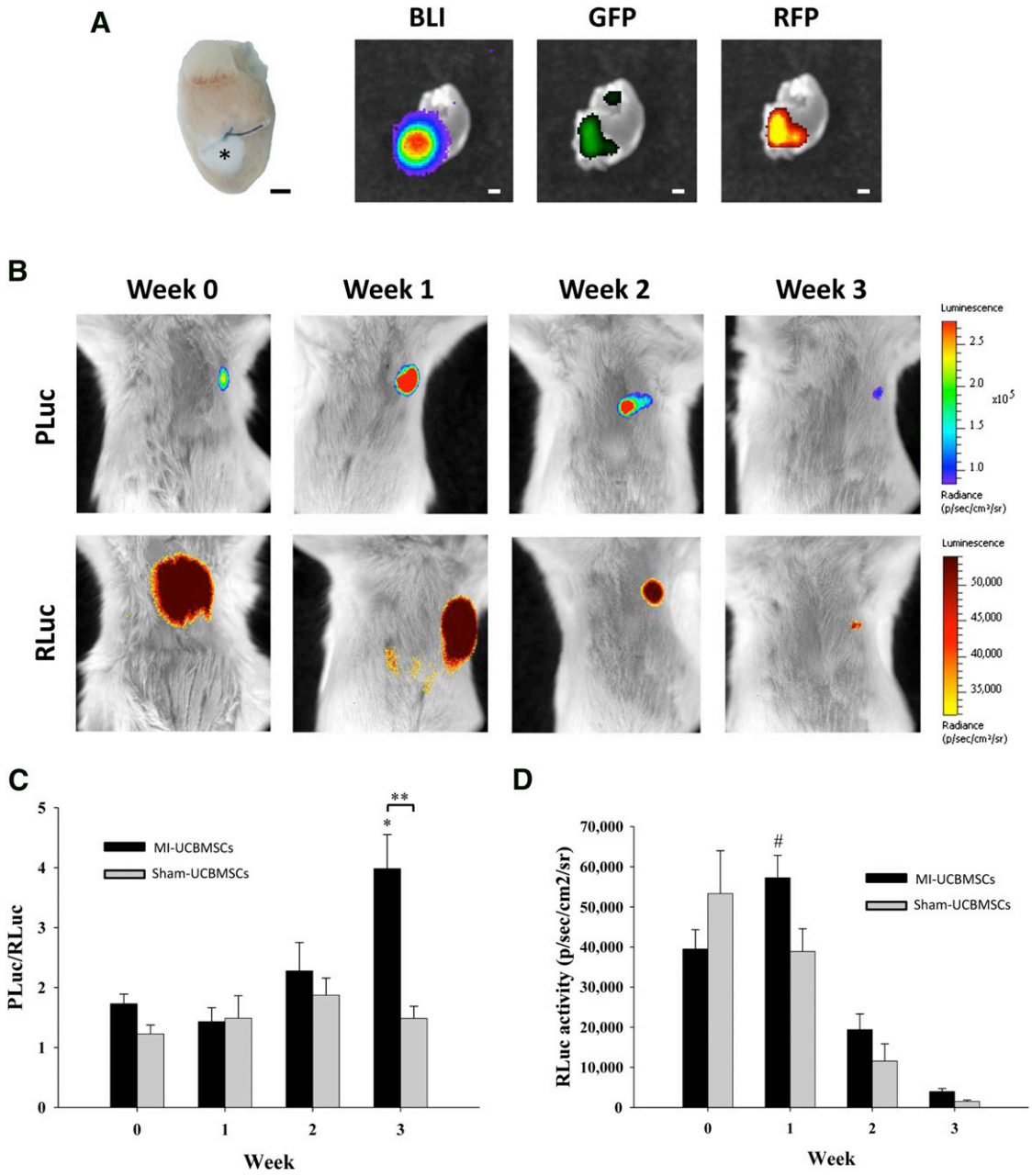

Figure 3. BLI of the three-dimensional engineered fibrin-cell patches implanted over infarcted myocardium wounds. **(A):** Representative photographs of a heart excised from a postinfarct mouse at 4 weeks after implantation of an adhesive fibrin-based patch composed of human UCBMSCs (asterisk) showing PLuc bioluminescence and eGFP and mRFP1 fluorescence emission. **(B):** BLI of PLuc (top) or RLuc (bottom) from the implanted UCBMSCs. Bioluminescence images are superimposed on black and white images of recipient mice. The color bars illustrate the relative light intensities from PLuc and RLuc (low, blue and yellow; high, red and black). Histograms show changes in the PLuc/RLuc ratio **(C)** and total RLuc activity **(D)**. ∗, $p = .003$ and #, $p = .045$ (relative to time of implantation), and ∗∗, $p < .001$. Scale bars = 1 mm. Abbreviations: BLI, bioluminescence imaging; eGFP, enhanced green fluorescent protein; PLuc, *Photinus pyralis* luciferase; RLuc, *Renilla reniformis* luciferase; p/s/cm^2/sr, photons per second per square centimeter per steradian; UCBMSCs, umbilical cord blood mesenchymal stem cells.

experience, most (~90%) double-labeled (eGFP and Luc) human adipose tissue-derived MSCs intramuscularly or intravenously implanted in immunocompromised mice either die or migrate away from the implantation site and are found (<1%) in the liver [36]. Thus, novel strategies, such as those based on tissue engineering procedures, are needed [6, 9, 10].

The transplantation of cellularized scaffolds or "patches" over the infarcted myocardium protects from cell loss after delivery to the sites of injury [19, 37, 38]. Currently, none of the biomaterials tested, whether synthetic or natural, have demonstrated optimal properties for cardiac tissue repair [9]. Fibrin, the naturally truncated form of fibrinogen, is already widely used in biomedical applications because of its ability to act as a biocompatible glue, holding cells in place and stimulating angiogenesis [39–43]. We used fibrin for the generation of a 3D adhesive patch filled with UCBMSCs. This patch was subsequently engrafted over the

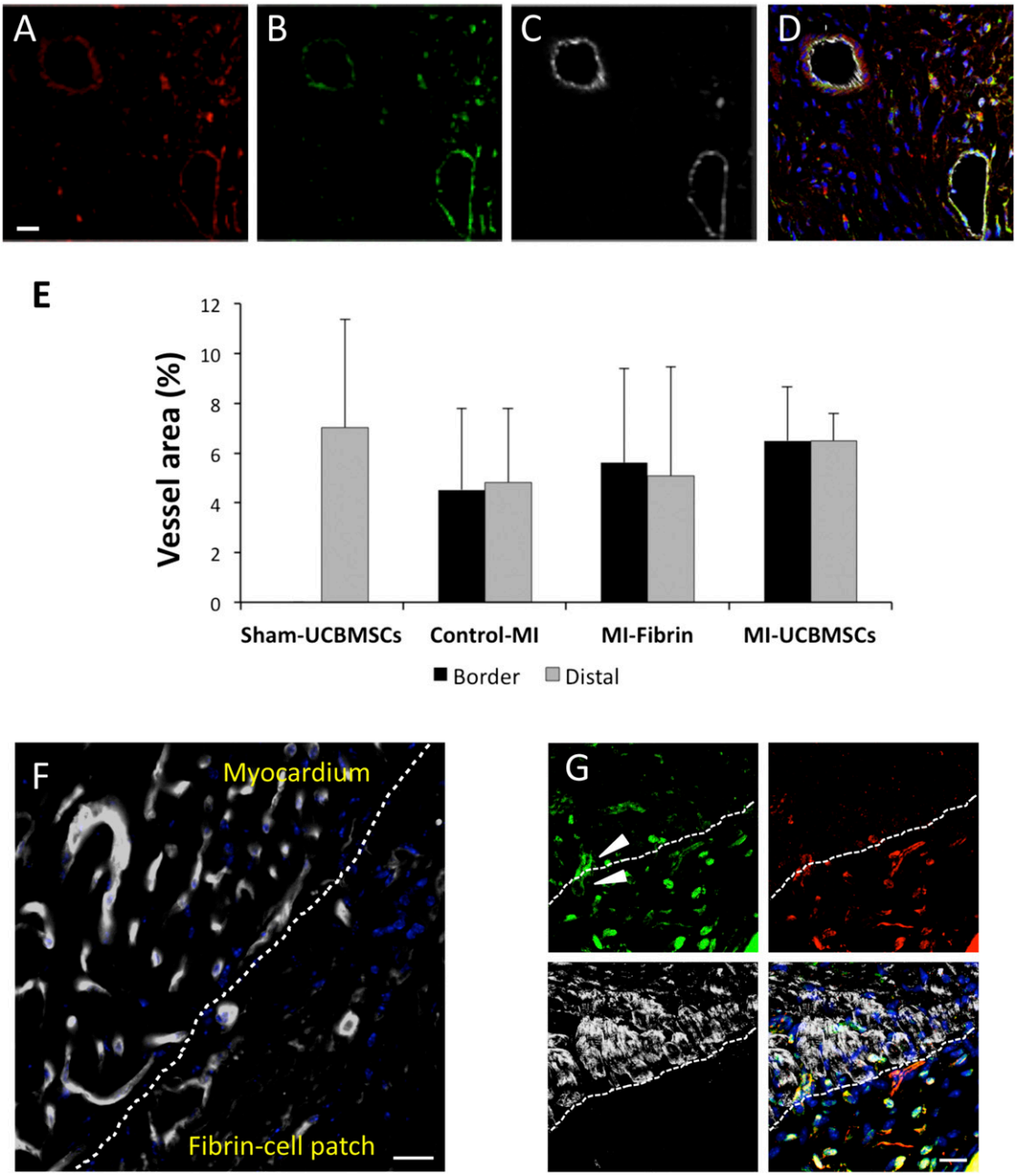

Figure 4. Detection of implanted UCBMSCs and functional vascular structures induced in the infarcted myocardium and fibrin-cell patch interface. **(A–C):** Representative fluorescence confocal microscope images of a 4-week-old fibrin-cell patch showing, from left to right, red fluorescent human UCBMSCs expressing cytomegalovirus promoter-regulated monomeric red fluorescent protein (mRFP1) **(A)**, green fluorescent UCBMSCs expressing CD31 promoter-regulated eGFP **(B)**, and cells expressing CD31 protein **(C)**. **(D):** Merged image of A, B, and C showing nuclei counterstained with Hoechst 33342. **(E):** Histogram showing the vessel density expressed as the percentage of the area occupied by GSLI $B4^+$ cells in sham-UCBMSC, control-MI, MI-fibrin, and MI-UCBMSC mice. **(F):** GSLI B4 staining (white) showing vessel-like structures within the fibrin-cell patch at 4 weeks after infarction. **(G):** Vascular structures at the interface (dashed line) between the subjacent infarcted myocardium wound and engrafted construct. Arrowheads indicate a representative functional microvessel filled with fluorescein isothiocyanate-dextran (green) traversing the interface between the host myocardium and cell-seeded fibrin patch (top left). Red fluorescent UCBMSCs expressing mRFP1 frequently populated the fibrin patch but not the subjacent myocardium (top right). Cardiomyocytes, labeled using a specific anti-cardiac troponin I antibody (white), exclusively populated the myocardial side of the interface (bottom left). Superimposition of the three images showed nuclei counterstained with Hoechst 33342 and yellow color stain, resulting from the superposition of red fluorescent UBCMSCs and green fluorescent dextran (bottom right). Scale bars = 20 μm. Abbreviations: control-MI, myocardial infarction induced but no treatment; eGFP, enhanced green fluorescent protein; MI-fibrin, myocardial infarction treated with fibrin alone; MI-UCBMSC, myocardial infarction treated with umbilical cord blood mesenchymal stem cells; Sham-UCBMSC, no myocardial infarction but implantation of fibrin-cell patch.

Table 1. Cardiac function values

Measure	Sham-UCBMSC			Control-MI			MI-fibrin			MI-UCBMSC		
	Baseline	After MI	30 Days	Baseline	After MI	30 Days	Baseline	After MI	30 Days	Baseline	After MI	30 Days
LVAWd (mm)	0.8 ± 0.1	0.9 ± 0.2	0.9 ± 0.1	0.9 ± 0.1	1.0 ± 0.3	1.0 ± 0.2	1.0 ± 0.3	0.9 ± 0.1	0.9 ± 0.3	1.0 ± 0.3	1.0 ± 0.2	0.9 ± 0.2
LVAWs (mm)	1.1 ± 0.2	1.0 ± 0.2	1.2 ± 0.2	1.1 ± 0.2	1.1 ± 0.2	1.3 ± 0.3	1.0 ± 0.2	1.3 ± 0.1	1.0 ± 0.2	1.3 ± 0.3	1.2 ± 0.1	1.2 ± 0.2
LVPWd (mm)	0.9 ± 0.2	0.9 ± 0.2	0.8 ± 0.1	0.9 ± 0.2	1.0 ± 0.1	0.9 ± 0.2	0.9 ± 0.3	1.1 ± 0.2	1.0 ± 0.1	0.8 ± 0.2	0.9 ± 0.2	0.9 ± 0.1
LVPWs (mm)	1.2 ± 0.2	1.3 ± 0.2	1.2 ± 0.1	1.2 ± 0.2	1.2 ± 0.2	1.0 ± 0.1	1.2 ± 0.3	1.3 ± 0.2	1.1 ± 0.1	1.2 ± 0.2	1.1 ± 0.2	1.1 ± 0.1
LVEDD (mm)	3.6 ± 0.3	3.2 ± 0.3	3.7 ± 0.2	3.3 ± 0.2	3.4 ± 0.2	3.8 ± 0.4	3.4 ± 0.3	3.4 ± 0.4	3.9 ± 0.2	3.3 ± 0.3	3.4 ± 0.4	3.8 ± 0.2
LVESD (mm)	2.3 ± 0.3	1.9 ± 0.3	2.4 ± 0.3	2.1 ± 0.3	2.5 ± 0.3	2.9 ± 0.4	2.3 ± 0.3	2.5 ± 0.3	3.0 ± 0.2	2.1 ± 0.4	2.4 ± 0.3	2.7 ± 0.2
LVFS (%)	34.3 ± 5.5	36.9 ± 3.4	34.7 ± 5.1	34.9 ± 5.2	28.4 ± 4.1	21.3 ± 5.2	37.6 ± 3.2	26.7 ± 4.8	22.5 ± 5.2	35.1 ± 6.4	27.7 ± 5.4	28.9 ± 4.3
LVEF (%)	66.6 ± 5.7	67.4 ± 4.5	64.2 ± 7.6	65.2 ± 7.1	56.2 ± 6.4	43.8 ± 9.0	68.9 ± 4.0	53.1 ± 7.4	45.8 ± 8.8	65.5 ± 7.9	56.3 ± 10.1	56.8 ± 8.8

Data presented as mean ± SD.

Abbreviations: control-MI, myocardial infarction induced but no treatment; LVAWd, left ventricular anterior wall diastole; LVAWs, left ventricular anterior wall systole; LVEDD, left ventricular end-diastolic dimension; LVEF, left ventricular ejection fraction; LVESD, left ventricular end-systolic dimension; LVFS, left ventricular fractional shortening; LVPWd, left ventricular posterior wall diastole; LVPWs, left ventricular posterior wall systole; MI-fibrin, myocardial infarction treated with fibrin alone; MI-UCBMSC, myocardial infarction treated with umbilical cord blood mesenchymal stem cells; Sham-UCBMSC, no myocardial infarction but implantation of fibrin-cell patch.

Table 2. Left ventricle ejection fraction and fractional shortening calculated as differentials between values at 30 days postoperatively and baseline

Group	ΔLVEF (%)	*p* value	ΔLVFS (%)	*p* value
MI-UCBMSC	−8.7 ± 8.8		−6.2 ± 7	
Control-MI	−21.4 ± 7.7	.02	−13.6 ± 5.1	.07
MI-fibrin	−23.1 ± 23	.006	−15.1 ± 5	.02

Data presented as differential ± SD. *p* values are referred to MI-UCBMSC group.

Abbreviations: control-MI, myocardial infarction induced but no treatment; ΔLVEF, change in left ventricular ejection fraction; ΔLVFS, change in left ventricular fractional shortening; MI-fibrin, myocardial infarction treated with fibrin alone; MI-UCBMSC, myocardial infarction treated with umbilical cord blood mesenchymal stem cells.

infarcted myocardium wound. Recent findings have shown preliminary beneficial effects of human UCBMSCs in the post-MI environment; however, these cells failed to migrate within the damaged myocardium [19].

In the present study, we implanted these 3D engineered constructs and evaluated whether functional vascular connections with the host myocardium were present as well as the global cardiac functional recovery. One of the crucial aspects of cardiac tissue engineering is to generate constructs with great integration over damaged myocardium. After the implantation procedure, the patch had adhered well to the heart, and the implanted cells induced the growth of blood vessels that connected the underlying myocardium and the construct and promoted reverse remodeling, which was detectable as a general recovery of cardiac function after MI. The delivered cells newly expressed CD31 protein (which was absent in the preimplanted cells) and self-organized within the engrafted fibrin-cell patch, forming vessel-like structures filled with high-molecular-weight FITC-dextran, which was injected through the lateral tail vein of the mice before sacrifice. We also showed that this newly formed microvasculature was functional and connected the fibrin-cell patch to both the subjacent myocardial tissue and the host circulatory system. In contrast, no cells from the patch crossed the interface with the underlying myocardium.

Noninvasive BLI demonstrated early proliferation and differentiation of the implanted cells within the construct in the MI-UCBMSC mice. In particular, the activity of the constitutive active promoter (RLuc) within implanted cells increased at week 1 relative to implantation but later progressively decayed to approximately 12% of the initial value. This activity measures the survival rate of the cells implanted over time. Although the number of cells in the sham mice declined gradually, the number of cells in the infarcted mice increased at the beginning, probably in response to signaling factors generated by the infarct wound. Such factors might be also responsible for induction of the endothelial phenotype observed by the increase in the PLuc/RLuc ratio. Subsequently, despite our implantation strategy substantially favoring cell retention compared with other conventional cell delivery approaches, a proportion of these cells died rapidly after implantation. A possible reason for this is that the grafted cells were not a uniform population; thus, only some of them were destined to differentiate toward the endothelial lineage, and the rest did not find the right environment to survive. Flow cytometric analysis, however, appears to indicate that the implanted cell

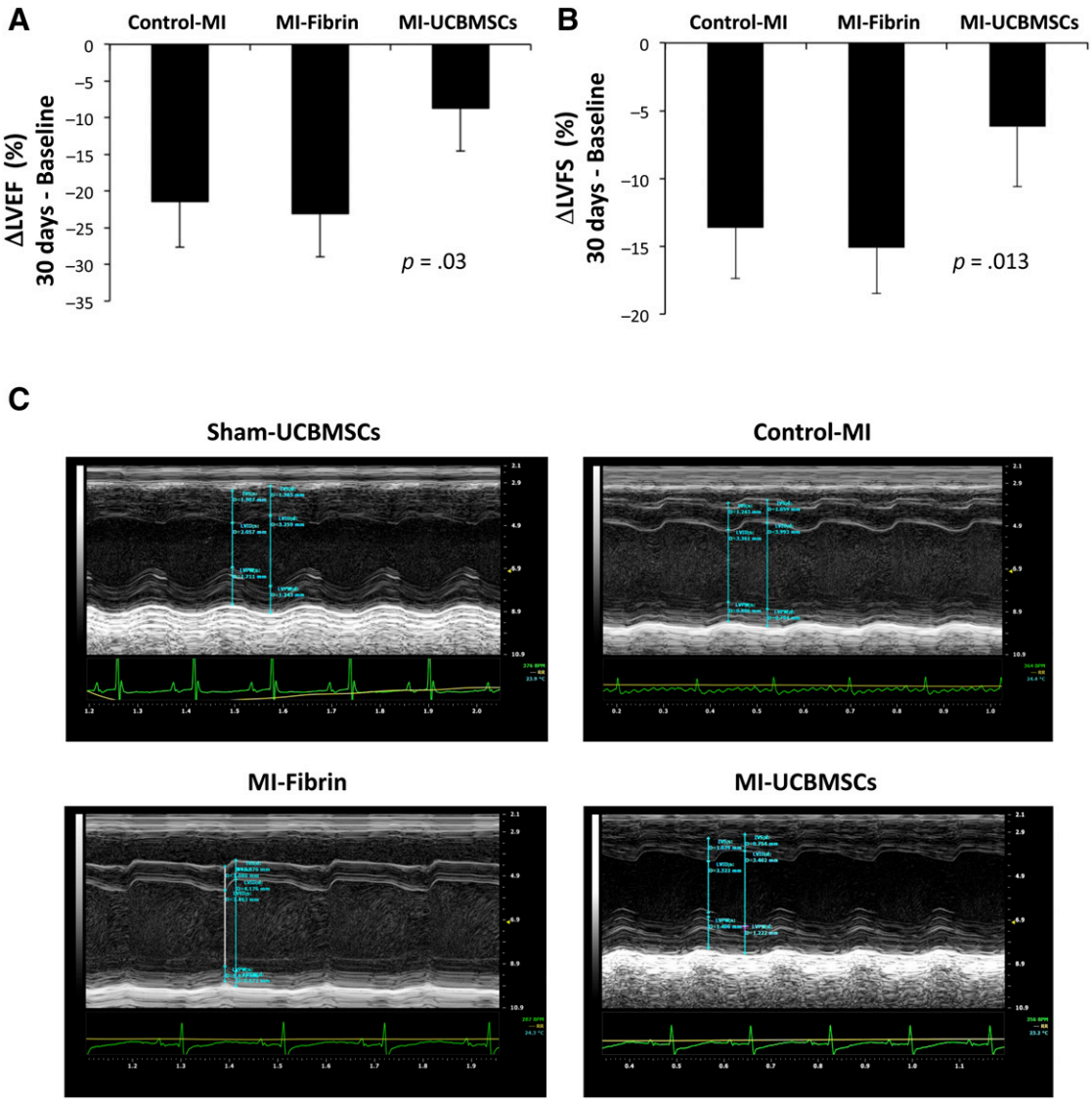

Figure 5. Echocardiographic evaluation of cardiac function. Histograms representing ΔLVEF **(A)** and ΔLVFS **(B)** from baseline to before sacrifice (30 days). Differences between groups were globally estimated using one-way analysis of variance. **(C):** Representative M-mode echocardiographic images in the parasternal long axis view. Abbreviations: control-MI, myocardial infarction induced but no treatment; ΔLVEF, change in left ventricular ejection fraction; ΔLVFS, change in left ventricular fractional shortening; MI-fibrin, myocardial infarction treated with fibrin alone; MI-UCBMSC, myocardial infarction treated with umbilical cord blood mesenchymal stem cells; Sham-UCBMSC, no myocardial infarction but implantation of fibrin-cell patch.

populations were robustly homogeneous because they did not contain cells that belonged to either the endothelial or hematopoietic cell lineages. Moreover, although we observed functional vessels induced in the infarcted myocardium and fibrin-cell patch interface, the implantation environment is generally not well irrigated and oxygen and nutrients are lacking right after implantation. This hypoxic state is a powerful driver of endothelial differentiation and promotes the selection of cells induced toward the endothelial lineage. In addition, it is not possible from in vivo BLI analysis alone to determine whether cell fusion was responsible for the increase in CD31-regulated light emission. However, although cell fusion events are controversial and at best rare, in our experiments, a remarkable increase occurred in the amount of light emitted by CD31-regulated luciferase relative to that produced by the internal control CMV-regulated luciferase. Although this would suggest that a large number of implanted cells would have to have fused with endogenous cells expressing CD31, we found this was very unlikely, in particular, because the patches were mainly populated by the implanted cells and no host cells were found in it.

Furthermore, the mice treated with the 3D engineered fibrin patch containing UCBMSCs exhibited a progressive increase in their contractile parameters compared with those treated with fibrin alone up to 4 weeks after implantation. These data are in agreement with data from previous studies, which demonstrated that an increased infarct wall thickness, using an acellular scaffold, was insufficient for preventing postinfarction LV remodeling [44–46]. Thus, our results suggest that additional multipotent UCBMSCs prevent such remodeling. Myocardial remodeling, as measured by the recovery of functional LV parameters to baseline

levels, was reversed when fibrin-UCBMSC patches were applied. In particular, the global beneficial effects of the fibrin-cell patch were not due to a local reduction in the infarct size; rather, they included remote effects on the noninfarcted myocardium and on the infarct/border areas. In support of this observation, a "systems biology" approach previously showed that acute MI induced substantial gene expression changes in remote myocardial regions in swine [47]. Furthermore, because many research efforts have focused on restoring myocardial damage after MI through cell therapy approaches, our findings should be interpreted with some considerations in respect to clinical significance. Because fibrin-cell patches were applied immediately after induction of the infarct, the potential benefits should be associated with mitigation rather than injury improvement.

Conclusion

We used a strategy based on the combination of noninvasive BLI and histological procedures, supported by the evaluation of cardiac functional parameters, to evaluate the benefits induced by a 3D fibrin-based patch, which was engineered as a UCBMSC support and transplanted locally over infarcted myocardium in mice. Compared with conventional strategies of cell administration, which have been associated with low cell survival, the construct used in our study conferred a favorable environment for cell viability and maintenance of the implanted cells at the myocardial infarct site, allowing them to exert effects for at least 3 weeks after implantation. Our system also has other benefits. The capacity to continually and noninvasively visualize the cellular processes and other biological interactions using BLI reduces the use of experimental animals and improves reproducibility. The use of luciferase reporters allows good quantification, because the correlation between the signal intensity and cell numbers is good [19, 48]. In our model, the correlational interpretation of the imaging and cardiac function data is complex. A tentative integrated interpretation of our data is that as patches with cells are implanted, the degradation of fibrin and the release of growth factors from dying and living cells produce an overall positive effect on the myocardium, observed as functional improvements. However, our results appear to indicate that the effects on cell proliferation, loss, and differentiation observed by BLI could decrease over time. The factors released by the cells, including those differentiating, might be responsible for sustained improvement in myocardial repair, in particular, in the vascular system. The implanted cells promoted and participated in the functional vascularization of the construct, but not of the subjacent or distal myocardial tissue, and did not significantly increase the infarct wall thickness or reduce scar volume. However, the infarcted mice treated with this fibrin-cell patch demonstrated postinfarction reverse remodeling that appeared as a general recovery of lost myocardial function.

Acknowledgments

We are indebted to the reviewers and editor for their invaluable advice. This work was supported by grants from Ministerio de Educación y Ciencia (Grants SAF2011-30067-C02-01 and SAF2012-33404), Fundació La MARATÓ de TV3 (Grant 122232), the European Commission 7th Framework Programme (REgeneration of CArdiac Tissue Assisted by Bioactive Implants; Grant NMP3-SL-2009-229239), Red de Terapia Celular (Grants RD12/0019/0029 and RD12/0019/0004), Red de Investigación Cardiovascular (Grant RD12/0042/0047), Sociedad Española de Cardiología, Societat Catalana de Cardiologia, and Fondo de Investigación Sanitaria, Instituto de Salud Carlos III (Grant FIS PI14/01682).

Author Contributions

S.R., C.S.-B., and J.R.B.: collection and assembly of data, data analysis and interpretation, manuscript writing; A.L.-V., M.A.F., C.G.-M., C.P.-V., and I.P.-G.: data analysis and interpretation; J.B. and A.B.-G.: conception and design, manuscript writing.

Disclosure of Potential Conflicts of Interest

J.B. has a compensated research contract with SAGETIS. The other authors indicated no potential conflicts of interest.

References

1 Pfeffer MA, Braunwald E. Ventricular remodeling after myocardial infarction. Experimental observations and clinical implications. Circulation 1990;81:1161–1172.

2 Kuhbier JW, Weyand B, Sorg H et al. [Stem cells from fatty tissue: A new resource for regenerative medicine?]. Chirurg 2010;81:826–832.

3 Hoke NN, Salloum FN, Loesser-Casey KE et al. Cardiac regenerative potential of adipose tissue-derived stem cells. Acta Physiol Hung 2009;96:251–265.

4 Orlic D, Kajstura J, Chimenti S et al. Transplanted adult bone marrow cells repair myocardial infarcts in mice. Ann N Y Acad Sci 2001;938:221–229.

5 Behfar A, Yamada S, Crespo-Diaz R et al. Guided cardiopoiesis enhances therapeutic benefit of bone marrow human mesenchymal stem cells in chronic myocardial infarction. J Am Coll Cardiol 2010;56:721–734.

6 Soler-Botija C, Bagó JR, Bayes-Genis A. A bird's-eye view of cell therapy and tissue engineering for cardiac regeneration. Ann N Y Acad Sci 2012;1254:57–65.

7 Lunkenheimer PP, Redmann K, Westermann P et al. The myocardium and its fibrous matrix working in concert as a spatially netted mesh: A critical review of the purported tertiary structure of the ventricular mass. Eur J Cardiothorac Surg 2006;29(suppl 1):S41–S49.

8 Vunjak-Novakovic G, Lui KO, Tandon N et al. Bioengineering heart muscle: A paradigm for regenerative medicine. Annu Rev Biomed Eng 2011;13:245–267.

9 Gálvez-Montón C, Prat-Vidal C, Roura S et al. Update: Innovation in cardiology (IV). Cardiac tissue engineering and the bioartificial heart. Rev Esp Cardiol (Engl Ed) 2013;66:391–399.

10 Soler-Botija C, Galvez-Monton C, Prat-Vidal C et al. Myocardial bioprosthesis: Mimicking nature. Drugs Future 2013;38:475–484.

11 Bagó JR, Aguilar E, Alieva M et al. In vivo bioluminescence imaging of cell differentiation in biomaterials: A platform for scaffold development. Tissue Eng Part A 2013;19:593–603.

12 Roura S, Gálvez-Montón C, Bayes-Genis A. Bioluminescence imaging: A shining future for cardiac regeneration. J Cell Mol Med 2013;17:693–703.

13 Drexler H, Hornig B. Endothelial dysfunction in human disease. J Mol Cell Cardiol 1999;31:51–60.

14 Maulik N, Thirunavukkarasu M. Growth factors and cell therapy in myocardial regeneration. J Mol Cell Cardiol 2008;44:219–227.

15 Roura S, Gálvez-Montón C, Bayes-Genis A. The challenges for cardiac vascular precursor cell therapy: Lessons from a very elusive precursor. J Vasc Res 2013;50:304–323.

16 Prat-Vidal C, Roura S, Farré J et al. Umbilical cord blood-derived stem cells spontaneously express cardiomyogenic traits. Transplant Proc 2007;39:2434–2437.

17 Roura S, Farré J, Hove-Madsen L et al. Exposure to cardiomyogenic stimuli fails to transdifferentiate human umbilical cord blood-derived mesenchymal stem cells. Basic Res Cardiol 2010;105:419–430.

18 Roura S, Pujal JM, Bayes-Genis A. Umbilical cord blood for cardiovascular cell therapy: From promise to fact. Ann N Y Acad Sci 2012; 1254:66–70.

19 Roura S, Bagó JR, Soler-Botija C et al. Human umbilical cord blood-derived mesenchymal stem cells promote vascular growth in vivo. PLoS ONE 2012;7:e49447.

20 Dégano IR, Vilalta M, Bagó JR et al. Bioluminescence imaging of calvarial bone repair using bone marrow and adipose tissue-derived mesenchymal stem cells. Biomaterials 2008;29: 427–437.

21 Vilalta M, Jorgensen C, Dégano IR et al. Dual luciferase labelling for non-invasive bioluminescence imaging of mesenchymal stromal cell chondrogenic differentiation in demineralized bone matrix scaffolds. Biomaterials 2009; 30:4986–4995.

22 Almendro N, Bellón T, Rius C et al. Cloning of the human platelet endothelial cell adhesion molecule-1 promoter and its tissue-specific expression. Structural and functional characterization. J Immunol 1996;157:5411–5421.

23 Davoli F, Sellitri F, Brandolini J et al. Use of coagulant spray glue (Glubran 2) for aerostatic purposes in pulmonary parenchyma resections in pigs: A preliminary study. Eur Surg Res 2009; 43:360–364.

24 Del Corso A, Bargellini I, Cicorelli A et al. Efficacy and safety of a novel vascular closure device (Glubran 2 seal) after diagnostic and interventional angiography in patients with peripheral arterial occlusive disease. Cardiovasc Intervent Radiol 2013;36:371–376.

25 Bayes-Genis A, Soler-Botija C, Farré J et al. Human progenitor cells derived from cardiac adipose tissue ameliorate myocardial infarction in rodents. J Mol Cell Cardiol 2010;49: 771–780.

26 Teichholz LE, Kreulen T, Herman MV et al. Problems in echocardiographic volume determinations: Echocardiographic-angiographic correlations in the presence of absence of asynergy. Am J Cardiol 1976;37:7–11.

27 Gálvez-Montón C, Prat-Vidal C, Roura S et al. Transposition of a pericardial-derived vascular adipose flap for myocardial salvage after infarct. Cardiovasc Res 2011;91:659–667.

28 Gálvez-Montón C, Prat-Vidal C, Roura S et al. Post-infarction scar coverage using a pericardial-derived vascular adipose flap. Preclinical results. Int J Cardiol 2013;166:469–474.

29 Murry CE, Reinecke H, Pabon LM. Regeneration gaps: Observations on stem cells and cardiac repair. J Am Coll Cardiol 2006;47:1777–1785.

30 Genovese J, Cortes-Morichetti M, Chachques E et al. Cell based approaches for myocardial regeneration and artificial myocardium. Curr Stem Cell Res Ther 2007;2:121–127.

31 Chachques JC. Cardiomyoplasty: Is it still a viable option in patients with end-stage heart failure? Eur J Cardiothorac Surg 2009;35: 201–203.

32 Chachques JC, Trainini JC, Lago N et al. Myocardial assistance by grafting a new bioartificial upgraded myocardium (MAGNUM trial): Clinical feasibility study. Ann Thorac Surg 2008; 85:901–908.

33 Assmus B, Schächinger V, Teupe C et al. Transplantation of progenitor cells and regeneration enhancement in acute myocardial infarction (TOPCARE-AMI). Circulation 2002; 106:3009–3017.

34 Barbash IM, Chouraqui P, Baron J et al. Systemic delivery of bone marrow-derived mesenchymal stem cells to the infarcted myocardium: Feasibility, cell migration, and body distribution. Circulation 2003;108:863–868.

35 Freyman T, Polin G, Osman H et al. A quantitative, randomized study evaluating three methods of mesenchymal stem cell delivery following myocardial infarction. Eur Heart J 2006;27:1114–1122.

36 Vilalta M, Dégano IR, Bagó J et al. Biodistribution, long-term survival, and safety of human adipose tissue-derived mesenchymal stem cells transplanted in nude mice by high sensitivity non-invasive bioluminescence imaging. Stem Cells Dev 2008;17:993–1003.

37 Suuronen EJ, Kuraitis D, Ruel M. Improving cell engraftment with tissue engineering. Semin Thorac Cardiovasc Surg 2008;20:110–114.

38 Xing Y, Lv A, Wang L et al. Engineered myocardial tissues constructed in vivo using cardiomyocyte-like cells derived from bone marrow mesenchymal stem cells in rats. J Biomed Sci 2012;19:6.

39 Amrani DL, Diorio JP, Delmotte Y. Wound healing. Role of commercial fibrin sealants. Ann N Y Acad Sci 2001;936:566–579.

40 Bensaïd W, Triffitt JT, Blanchat C et al. A biodegradable fibrin scaffold for mesenchymal stem cell transplantation. Biomaterials 2003; 24:2497–2502.

41 Christman KL, Vardanian AJ, Fang Q et al. Injectable fibrin scaffold improves cell transplant survival, reduces infarct expansion, and induces neovasculature formation in ischemic myocardium. J Am Coll Cardiol 2004;44:654–660.

42 Leor J, Amsalem Y, Cohen S. Cells, scaffolds, and molecules for myocardial tissue engineering. Pharmacol Ther 2005;105:151–163.

43 Ahmed TA, Dare EV, Hincke M. Fibrin: A versatile scaffold for tissue engineering applications. Tissue Eng Part B Rev 2008;14:199–215.

44 Lu WN, Lü SH, Wang HB et al. Functional improvement of infarcted heart by co-injection of embryonic stem cells with temperature-responsive chitosan hydrogel. Tissue Eng Part A 2009;15:1437–1447.

45 Rane AA, Chuang JS, Shah A et al. Increased infarct wall thickness by a bio-inert material is insufficient to prevent negative left ventricular remodeling after myocardial infarction. PLoS One 2011;6:e21571.

46 Garbern JC, Minami E, Stayton PS et al. Delivery of basic fibroblast growth factor with a pH-responsive, injectable hydrogel to improve angiogenesis in infarcted myocardium. Biomaterials 2011;32:2407–2416.

47 Prat-Vidal C, Gálvez-Montón C, Nonell L et al. Identification of temporal and region-specific myocardial gene expression patterns in response to infarction in swine. PLoS One 2013;8:e54785.

48 Close DM, Xu T, Sayler GS et al. In vivo bioluminescent imaging (BLI): Noninvasive visualization and interrogation of biological processes in living animals. Sensors (Basel) 2011; 11:180–206.

See www.StemCellsTM.com for supporting information available online.